In Vitro Flow Analysis of a Patient-Specific Intraatrial Total Cavopulmonary Connection

Diane A. de Zélicourt, MS, Kerem Pekkan, PhD, Lisa Wills, BS, Kirk Kanter, MD, Joseph Forbess, MD, Shiva Sharma, MD, Mark Fogel, MD, and Ajit P. Yoganathan, PhD

Wallace H. Coulter Department of Biomedical Engineering, Georgia Institute of Technology and Emory University, Departments of Surgery and Pediatric Cardiology, Emory University, Atlanta, Georgia, and Division of Cardiology, The Children's Hospital of Philadelphia, Philadelphia, Pennsylvania

Background. **Understanding the hemodynamics of the total cavopulmonary connection may lead to further optimization of the connection design and surgical planning, which in turn may lead to improved surgical outcome. Although most experimental and numerical investigations have mainly focused on somewhat simplified geometries, investigation of the flow field of true anatomic configurations is necessary for a true understanding.**

Methods. **An intraatrial connection was reconstructed from patient magnetic resonance images and manufactured using transparent stereolithography. Power loss, flow visualization, and digital particle image velocimetry as well as computational fluid dynamics simulations were performed to characterize the anatomic flow structure. Given the complexity of the anatomic flow, two simplified versions of the geometry were manufactured and run through power loss and flow visualization studies.**

Results. **Experimental measurements revealed complex, unsteady, and highly three-dimensional flow structures within the anatomic model, leading to high pressure drops and power losses. The small vessel diameters were the primary cause of these losses. Numerical simulations demonstrated that most of the dissipation occurred in the pulmonary arteries. Finally, asymmetric pulmonary diameters together with the bulgy intraatrial connection favored the rise of flow unsteadiness and unbalanced lung perfusion.**

Conclusions. **The technique developed in this study enabled a deeper understanding of the hemodynamics behind an intraatrial connection. Future endeavors would be to study variation among differing surgical techniques, comparing intraatrial and extracardiac approaches.**

(Ann Thorac Surg 2005;79:2094–102)

Since its inception, modifications of the Fontan procedure [1] brought postoperative mortality down to the level of simpler congenital heart defect repairs. However, the marked improvement in surgical outcome is balanced by numerous and serious long-term complications encountered by patients undergoing Fontan procedures, such as ventricular dysfunction, thromboembolism, arrhythmias, or protein-losing enteropathy [2]. Among the multiple variables that determine the outcome and the quality of life of these patients, one that allows for some degree of control is the surgically created design of the bypass connection. Since the first in vitro experiment performed by de Leval and colleagues [3], understanding the hemodynamics at the connection site to optimize the connection design has been a major concern. In the current Fontan procedure, the total cavopulmonary connection (TCPC), the superior (SVC) and inferior (IVC) venae cavae are anastomosed in stages onto the pulmonary arteries (PAs) in a cross-shaped connection. Parametric in vitro and computational fluid dynamic (CFD) studies have been performed on idealized and simplified models [4–6]. Developments in numerical capabilities have led to more realistic modeling of the TCPC connection [7, 8] and confirmed the importance of the connection geometry on its efficiency. However, there has not been any study performed on an accurate replica of a TCPC involving both experimental and numerical studies.

The TCPC morphology is complex, with multiple geometric variables, owing to various patient physiologies as well as to different surgical procedures. The last stage of the TCPC alone, in which the IVC is connected to the PAs, is subject to multiple approaches resulting in drastically different geometries, which are expected to yield very different flow fields. Intraatrial tunnels, for example, in which part of the atrial wall is used to extend the IVC up to the PAs and provide some growth potential to the connection, often result in bulgy connection areas. Extracardiac tunnels, in which the IVC is extended using a synthetic graft going around the heart, usually result in smoother geometries that are expected to yield smoother flow fields.

The present study aims at providing a deeper understanding of the hemodynamics behind physiologic TCPC configurations. It features an intraatrial TCPC morphol-

Accepted for publication Dec 28, 2004.

Address reprint requests to Dr Yoganathan, Wallace H. Coulter Department of Biomedical Engineering, Georgia Institute of Technology and Emory University, Room 2119 U.A. Whitaker Building, 313 Ferst Dr, Atlanta, GA 30332-0535; e-mail: ajit.yoganathan@bme.gatech.edu.

Published by Elsevier Inc

0003-4975/05/$30.00
doi:10.1016/j.athoracsur.2004.12.052

ogy that was reconstructed from the chest magnetic resonance imaging of a 13-year-old Fontan patient and uses rapid-prototyping with the recently available transparent stereolithographic resins for the construction of anatomically accurate experimental models. Two additional simplified glass models are also studied in an effort to better understand the complex anatomic flow.

Material and Methods

Anatomic Intraatrial Model

Twenty T_1-weighted axial magnetic resonance images were acquired covering the connection region of a 13-year-old Fontan patient who was born with a hypoplastic left heart syndrome and had undergone a hemi-Fontan at the age of 6 weeks, followed by an intraatrial TCPC procedure at the age of 17 months. The TCPC blood volume (Fig 1A) was reconstructed from the magnetic resonance imaging data and used to generate both the numerical mesh and the experimental model. To avoid the laborious casting processes [9], the design was inverted within a computer-aided design software package, I-DEAS 9.0 (EDS, Plano, TX), and the experimental model was manufactured using the rapid-prototyping technology with a transparent resin, Vantico Renshape 5510 (Renshape Solutions, Cambridge, UK). As computer-aided design data may also be directly exported for CFD grid generation, this methodology, which is further detailed by de Zélicourt and associates [10], results in identical experimental and numerical models that replicate the patient's anatomy within 0.7 mm with the resolution of our magnetic resonance imaging and rapid-prototyping hardware.

Simplified Glass Models

The two additional simplified glass models that were manufactured were designed as an extension of earlier parametric studies and meant to isolate the impact of the large connection area and of the small vessel dimensions, with a left pulmonary artery (LPA) smaller than the right pulmonary artery (RPA).

Model 1 (Fig 1B) reproduced the anatomic vessel diameters used by Ryu and coworkers [5] and Liu and associates [6], namely 8 mm, 13.3 mm, and 15 mm for the SVC, the PAs, and the IVC, respectively. The vessels were flared at the anastomosis site. The radius of curvature at the connection was equal to the radius of the connecting vessel. Although both of the above studies included a caval offset and a smooth connection area, model 1 featured no caval offset and a large connection area that reproduced the hydraulic diameter of the anatomic model, 18 mm.

Model 2 (Fig 1C) was identical to model 1 except for the vessel diameters that reproduced the hydraulic diameters of the anatomic model 1 cm away from the connection, namely 13.3 mm, 5 mm, 5 mm, and 8 mm for the IVC, SVC, LPA, and RPA, respectively.

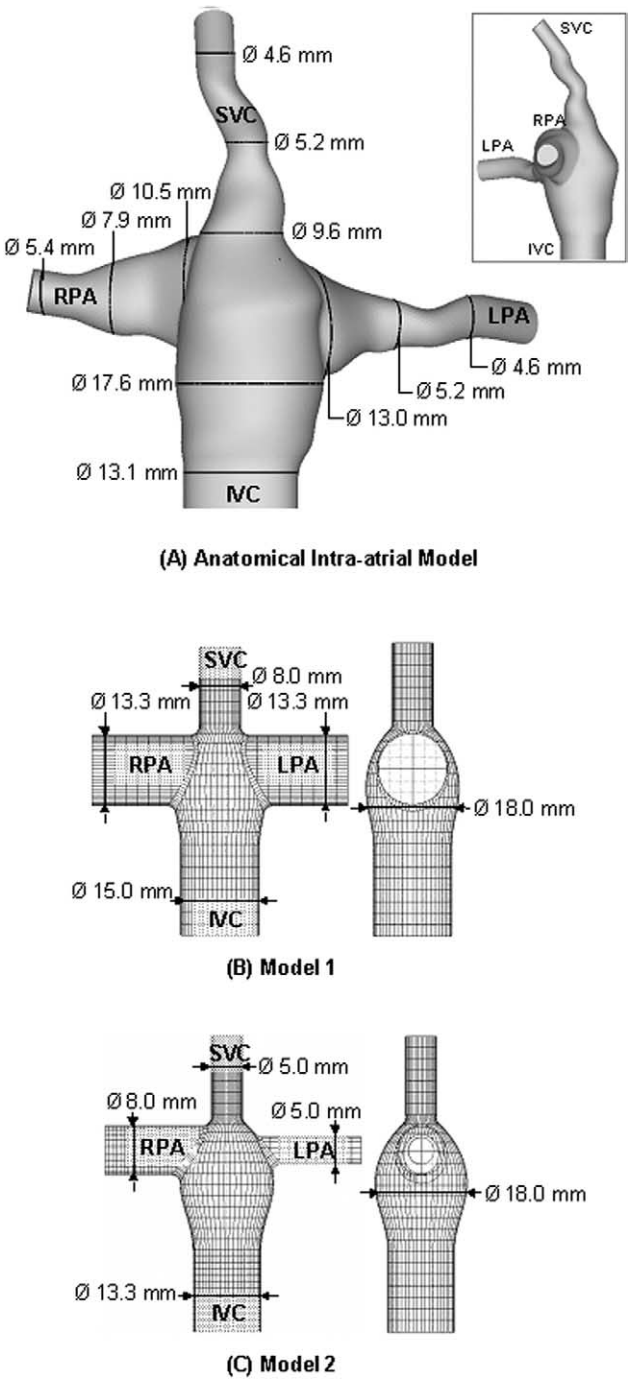

Fig 1. The anatomic intraatrial model reconstructed from magnetic resonance imaging (A) and the two simplified glass models (B and C). (IVC = *inferior vena cava;* LPA = *left pulmonary artery;* RPA = *right pulmonary artery;* SVC = *superior vena cava;* Ø = *diameter.*)

Flow Loop and Instrumentation

All experiments were conducted under steady inflow conditions. Total cardiac output ranged from 1 to 3 L/min. Additional runs at 4 L/min were performed on model 1 to enable the comparison with previous studies

on similar geometries [6]. The SVC/IVC flow ratio was fixed at 40/60 to reflect the flow splits seen in older children, whereas the RPA/LPA ratio was varied from 30/70 to 70/30 by 10% increments to simulate variable pulmonary flow splits. A solution of water–glycerin reproduced the kinematic viscosity of blood (v = 3.5 cSt ± 0.1 cSt). Sodium iodide was added to match the refractive index of the stereolithographic resin (n = 1.51) for the digital particle image velocimetry studies.

Hydrodynamic Power Loss

Holes were taped into the tubing extension of each vessel 10 cm away from the center of connection. Differential static pressures were acquired at each location with reference to the IVC. Twenty-four independent measurements were taken for each flow condition. They were corrected for pressure head bias and then used to compute power losses across the connection using an integrated, control-volume energy balance [11]:

$$E_{Loss} = \sum_{Inlets} P_i \cdot Q_i - \sum_{Outlets} P_i \cdot Q_i \qquad (1)$$

where P_i and $\dot{Q}_i$, respectively, are the corrected static pressure and the volumetric flow rate in each vessel. The 24 power loss values obtained for each flow condition were averaged into a single data set with the corresponding standard deviation.

Equal Pulmonary Vascular Resistance

In a patient, the pulmonary flow split is imposed by the resistance encountered by the blood as it goes through the lungs. To assess the quality of the lung perfusion associated with each TCPC design a simple lump parameter model was implemented to incorporate the pulmonary vascular resistance (PVR). Given the small size of the capillaries, the linear Darcy's model holds for the capillary lung flows:

$$R_{Left} \cdot Q_{LPA} = P_{LPA} - P_{PV} \qquad (2)$$

$$R_{Right} \cdot Q_{RPA} = P_{RPA} - P_{PV} \qquad (3)$$

where R_{Left} and R_{Right} are the left and right lung resistances, $\dot{Q}_{LPA}$ and $\dot{Q}_{RPA}$ are the flow rates through the LPA and the RPA, and P_{LPA}, P_{RPA}, and P_{PV} are the pressures in the LPA, RPA, and in the pulmonary venous return. Subtracting equation 3 from equation 2, we obtain the following relation:

$$R_{Right} \cdot \left(\frac{R_{Left}}{R_{Right}} Q_{LPA} - Q_{RPA} \right) = P_{LPA} - P_{RPA} \qquad (4)$$

The difference in pressure between the two pulmonary artery branches, $P_{LPA} - P_{RPA}$, is known from the experimental measurements as a function of flow split, $\dot{Q}_{RPA}/\dot{Q}_{LPA}$. Equation 4 can thus be solved with respect to the pulmonary flow split. The solution provides the amount of blood going to the left and right lung when the TCPC under study is coupled with the two PVR values R_{Left} and R_{Right}. In this study, we assumed both lungs to have a similar resistance: R_{Left} and R_{Right} were set to an average PVR value of 1.8 Wood units.

Velocity Field Characterization

Qualitative flow visualization was performed on all models by injecting a mixture of soap and dry pigments into the venae cavae. A high-speed digital camera (Basler A504k, Basler AG Vision Components, Ahrensburg, Germany) captured the streak lines at 500 frames/s. Two-dimensional digital particle image velocimetry was performed using a TSI system (TSI Inc, Shoreview, MN) on the anatomic model only. Velocity data were acquired in the sagittal direction. Three hundred paired frames were acquired at each location. The velocity fields were then computed and averaged using DaVis 6.2.2 (LaVision Gmbh, Gottingen, Germany) software.

Numerical Simulations

Computational fluid dynamic simulations were carried out with the commercial CFD package FIDAP (Fluent Inc, Lebanon, NH) concurrently to the experiments and run under the same conditions and assumptions as the experimental setup, namely incompressible, laminar flow with steady inflow conditions and rigid vessel walls. The first-order accurate CFD solutions of FIDAP agreed well with time-averaged experimental flow fields and control-volume power loss measurements. Grid generation, mesh refinement, numerical verification, and validation efforts are further detailed by Pekkan and colleagues [12].

Results

Model 1

Previous studies [4, 11] have demonstrated that the absence of caval offset leads to increased flow disturbance. In model 1 (Figs 2a, 2b), the caval flows collided in the center of the connection. The flow then swirled helically toward the PAs. Depending on the pulmonary flow split, the caval flows were directed preferably toward the left or the right side of the connection.

The losses observed in model 1 (Fig 3) were on the same order of magnitude as those observed by Ryu and colleagues [6] for the same vessel diameters. At all flow rates, minimum losses occurred at 50/50 RPA/LPA, whereas maximum losses were observed at both 30/70 and 70/30 RPA/LPA. Because of the symmetry of the model, the power losses had a symmetric behavior with respect to the pulmonary flow splits. Subsequently, the equal PVR point was 50/50 RPA/LPA.

Model 2

In model 2, the colliding caval flows no longer generated a stagnation region. Instead, the SVC flow went down into the connection, initiating an important clockwise recirculation throughout the entire connection that distributed the flow to the two PAs (Figs 2C, 2D). After recirculating throughout the pouch, the two caval flows were split between the LPA and RPA. As more flow was directed toward the RPA, the vortex lost strength and moved toward the LPA. At 70/30 RPA/LPA, the vortex could not be clearly identified. In its place, minor flow instability took place along the left wall of the connection,

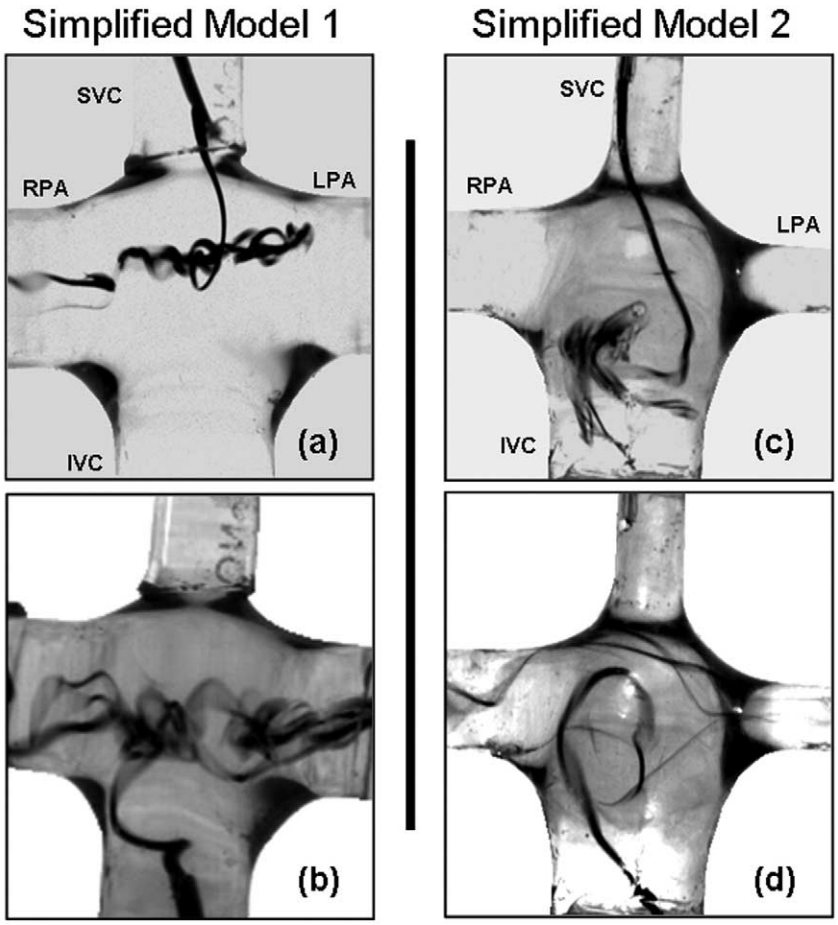

Fig 2. Flow visualization of the simplified glass models at 4 L/min for model 1 (a, b) and 1 L/min for model 2 (c, d); inflow split, 60/40 inferior vena cava (IVC) to superior vena cava (SVC); outflow split, 50/50 left pulmonary artery (LPA) to right pulmonary artery (RPA). Dye injected from the superior vena cava (top) and inferior vena cava (bottom).

although most of the flow went directly into the RPA. Finally, because of the bulgy aspect of the connection, the mixing of the caval flows was not two- but rather three-dimensional through all flow conditions. The high-velocity flow coming out of the SVC pushed the IVC stream toward either the anterior or the posterior side of the connection leading to three-dimensional mixing before entering the PAs with a helical pattern.

The losses observed in model 2 were one order of magnitude higher than those observed in model 1 and were highly dependent on the pulmonary flow ratio (Fig 4). Minimal losses occurred at 70/30 RPA/LPA, and were 55% to 65% lower than those measured at 30/70 RPA/LPA. At 3 L/min, when more than 50% of the flow was directed through the LPA, the flow in the LPA was turbulent (Reynolds number $>$ 2,300). The RPA flow remained in the laminar regimen throughout all flow conditions. The equal PVR point no longer corresponded to a 50/50 RPA/LPA flow split irrespective of the total flow rate; instead, it corresponded to a 62/38 RPA/LPA flow split at 1 L/min and went to an even more unbalanced flow split of 70/30 RPA/LPA at 2 and 3 L/min.

Anatomic Intraatrial Model

ANATOMY. The characteristic dimensions of the intraatrial TCPC (Fig 1A) were considerably smaller than what had previously been studied in the TCPC literature [5, 6]: the hydraulic diameters 2 cm away from the connection area were only 5.4 mm, 4.6 mm, 4.6 mm, and 13.1 mm for the RPA, LPA, SVC, and IVC, respectively. There was no caval offset. The central connection area, which had a hydraulic diameter of 18 mm, was larger than any of the connecting vessels. The vessels were flared toward the connection site: typically the LPA diameter ranged from 13.0 mm at the anastomosis site down to 5.2 mm and 4.6 mm, 1 cm and 2 cm downstream of the connection, respectively. In the same manner, the SVC and RPA connected to the pouch with a hydraulic diameter of 9.6 mm and 10.5 mm, respectively, but quickly tapered down to the dimensions previously mentioned. Finally, all four vessels were not coplanar. Although both the IVC and RPA stood in the coronal plane, the SVC and LPA bent toward the posterior side.

FLOW STRUCTURE. Despite the steady inflow conditions, flow visualization revealed highly unstable three-dimensional flow structures within the anatomic connection. These instabilities may be observed going through the series of snapshots taken at 1 L/min (Fig 5). At higher flow rates (3 L/min), the unsteadiness was too intense to properly visualize the flow.

As is further discussed by Pekkan and coworkers [12],

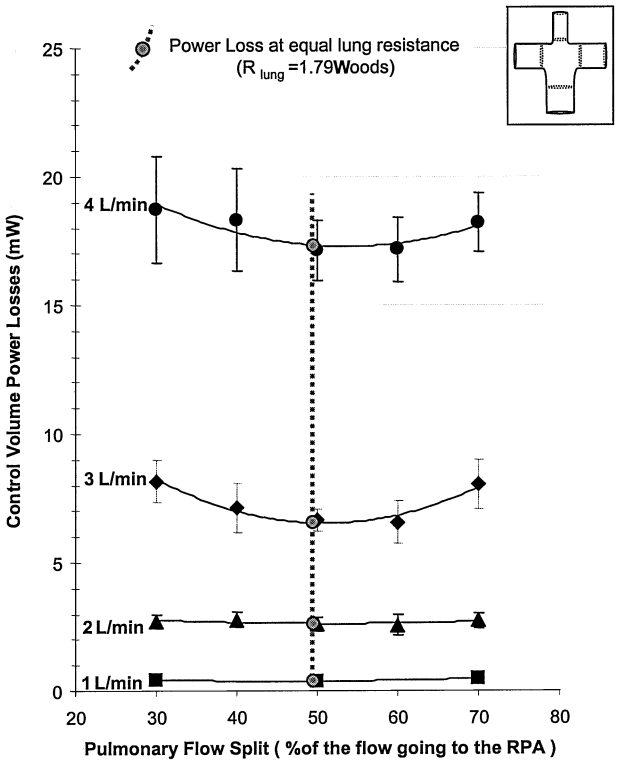

Fig 3. Control volume power losses in model 1, at 1, 2, 3, and 4 L/min, with a 60/40 inferior vena cava to superior vena cava flow split. (R_{lung} = lung resistance; RPA = right pulmonary artery.)

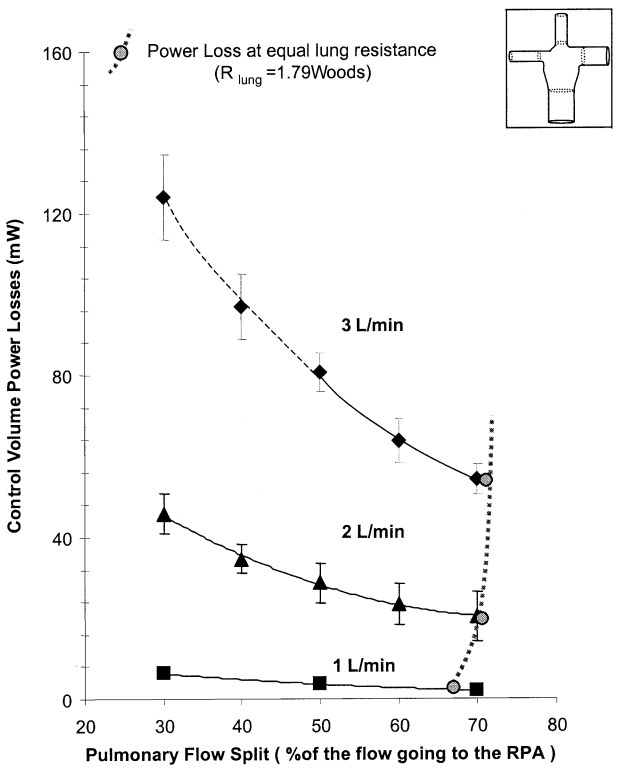

Fig 4. Control volume power losses in model 2, at 1, 2 and 3 L/min, with a 60/40 inferior vena cava to superior vena cava flow split. (R_{lung} = lung resistance; RPA = right pulmonary artery.)

the averaged CFD and digital particle image velocimetry results were in close agreement (Fig 6) and were used to obtain quantitative flow information. Because of optical limitations, only two-dimensional sagittal velocity fields could be acquired using the digital particle image velocimetry system. The validated CFD results were used to provide the total velocity magnitude (including all three velocity components) in the sagittal planes previously imaged, as well as in the coronal and axial directions (Fig 7).

Quantitative and qualitative findings are summarized in Figure 8. The SVC flow was three times faster than the IVC flow, and the LPA stream two times faster than the RPA stream for an equal share of the flow. The high-energy SVC stream was directed toward the anterior wall of the pouch and went far down into the connection area, generating a clockwise recirculation. The flow toward the posterior wall showed less disturbance and was dominated by the IVC flow. At the 70/30 RPA/LPA flow split, a highly unstable stagnation point was observed between the SVC and RPA anastomosis site. The caval flows entered the PAs either directly or after a thorough mixing, which filled up the pouch with streak traces. At other moments, caval flows would first flow into the stagnant SVC region and then reenter the pouch and flow into the PAs. At the 30/70 RPA/LPA flow split, the stagnation point could not be clearly identified. Mixing and flow disturbances could still be observed along the anterior wall. The IVC flow went along the posterior side into the LPA with little or no disturbance. Pulmonary artery flow was characterized by a helical pattern.

POWER LOSSES. Figure 9 displays the experimental power losses for 1, 2, and 3 L/min. They were two orders of magnitude higher than those observed in model 1 and only twice as high as in model 2. Similarly to model 2, they demonstrated a high sensitivity to pulmonary flow split, increasing at an always faster rate as the amount of the flow going to the RPA decreased. Minimum losses were observed when 60% to 70% of the flow was directed into the RPA and were 30% to 40% lower than those occurring at a 30/70 RPA/LPA flow split for the same total cardiac output.

For flow regimen assessment, Reynolds numbers (Re) were computed on the basis of the hydraulic diameters 2 cm away from the connection. Caval flow remained in the laminar regimen for all flow rates ($Re < 1{,}800$). At 3 L/min, LPA flow became turbulent ($Re > 2{,}300$) when 50% of the total flow or more was directed to the LPA. Similarly, the RPA flow became turbulent at 3 L/min when more than 60% of the flow was directed to the RPA. The pulmonary flow splits at which the PA flow is turbulent are represented with a dashed line in Figure 9. They correspond to those at which the data distribution was wider as a result of unsteady flow conditions in the PAs.

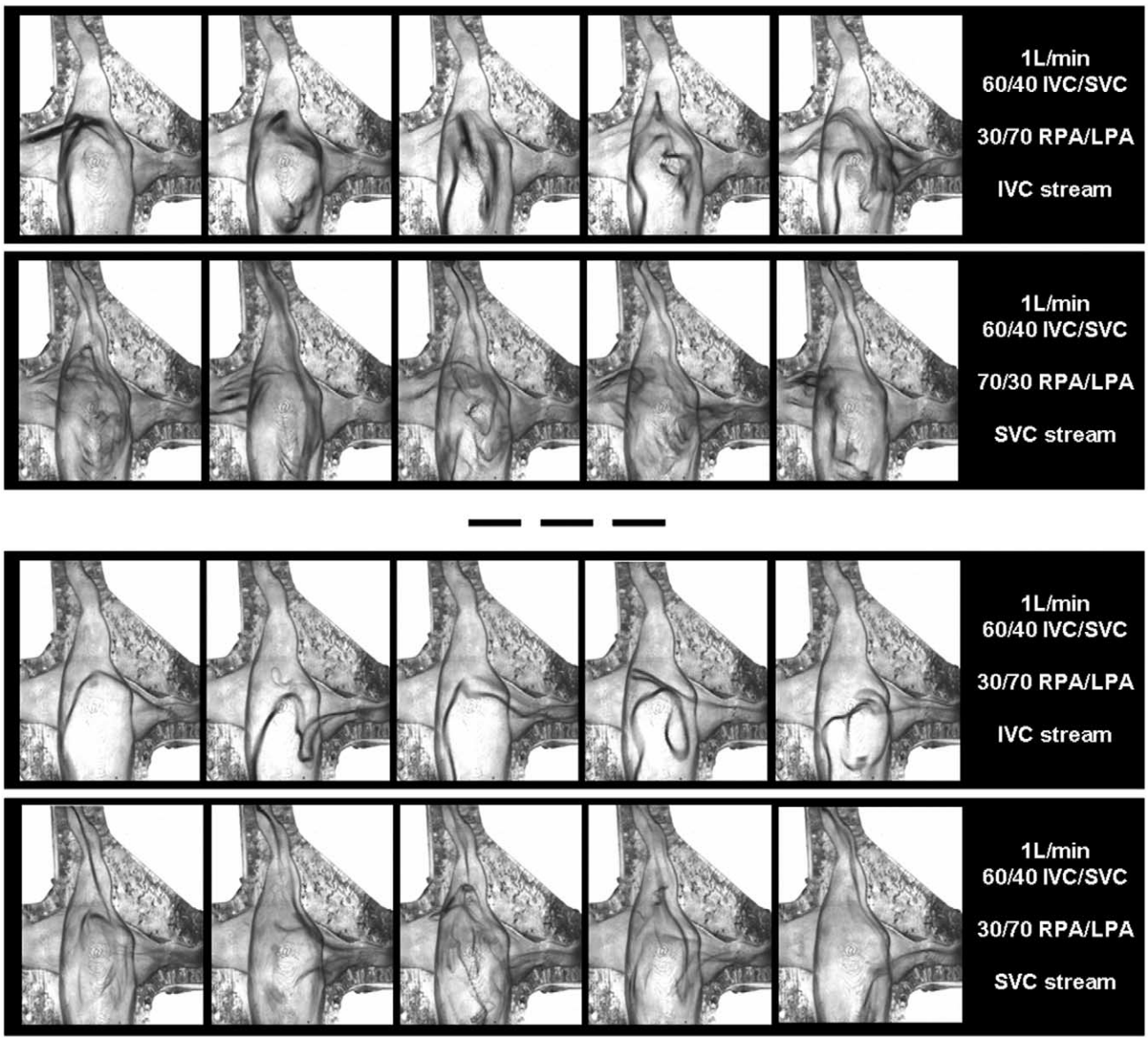

*Fig 5. Flow visualization of the intraatrial model at 1 L/min. (*IVC = *inferior vena cava;* LPA = *left pulmonary artery;* RPA = *right pulmonary artery;* SVC = *superior vena cava.)*

Comment

As has been summarized in the results section, the absence of caval offset in the anatomic intraatrial model resulted in important flow disturbance, which was enhanced by the large connection area. The smaller dimensions and the faster tapering of the LPA led to an unbalanced lung perfusion that favored RPA flow. The corresponding losses were two orders of magnitude higher than those observed in simpler glass models (model 1) and demonstrated a high sensitivity to pulmonary flow split.

The absence of caval offset combined with the pouch-like connection was modeled in model 1, inducing a 30% to 40% increase in power losses when compared with the ideal connection designed by Ryu and associates [6] for the same vessel diameters. The absence of caval offset increased the flow disturbance [4, 11, 13]. In the anatomic model, these flow instabilities were exacerbated by the complexity of the geometry. The wider connection site provided an extra degree of freedom, and three-dimensional flow patterns appeared where the caval flows collided. Additionally the diameter mismatch between the connection area and the connecting vessels increases the amount of flow separation and thus the energy dissipation.

Ryu and colleagues [6] found that changing the curvature of the PAs had less of an impact on the power losses than varying the diameters of the venae cavae. Similarly here, the aforementioned 30% to 40% increase in power losses caused by a suboptimal design of the connection

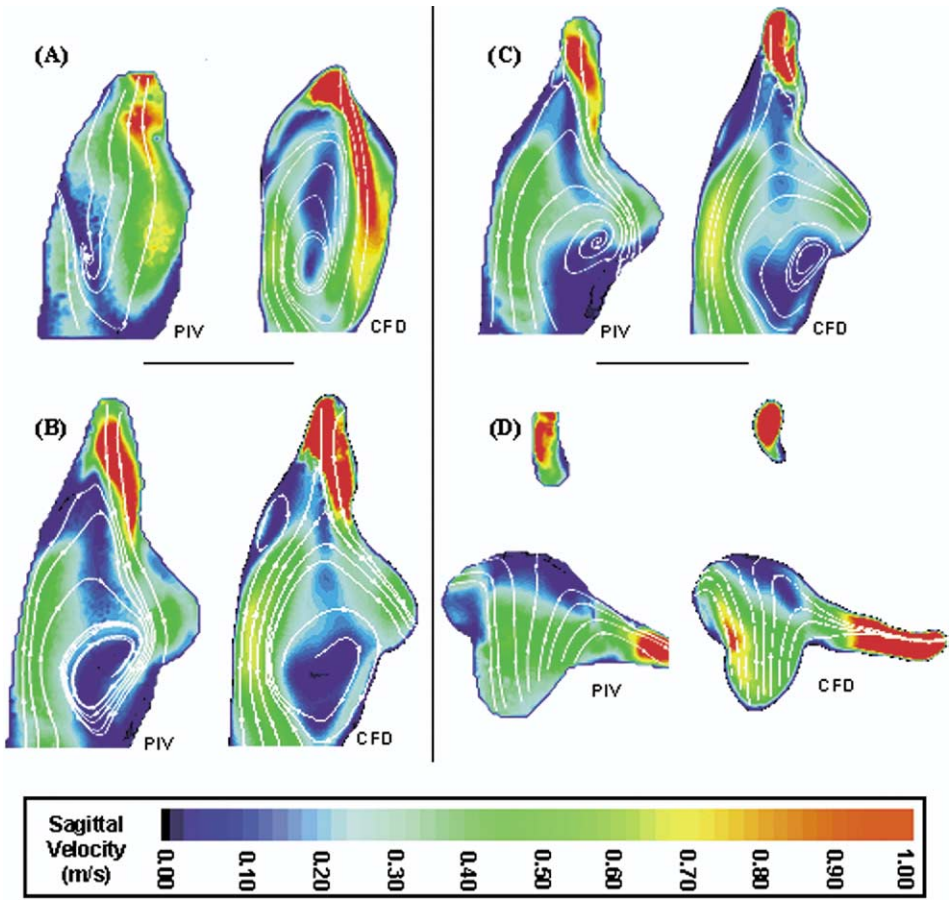

Fig 6. Quantitative assessment of the flow field using digital particle image velocimetry (PIV) and computational fluid dynamic (CFD) methods. Flow conditions: 3 L/min, 60/40 inferior vena cava to superior vena cava, and 50/50 left pulmonary artery to right pulmonary artery. The sagittal velocity maps are indexed from the most anterior plane (A) to the most posterior plane (D). The location of the sagittal planes is shown in Figure 7(1).

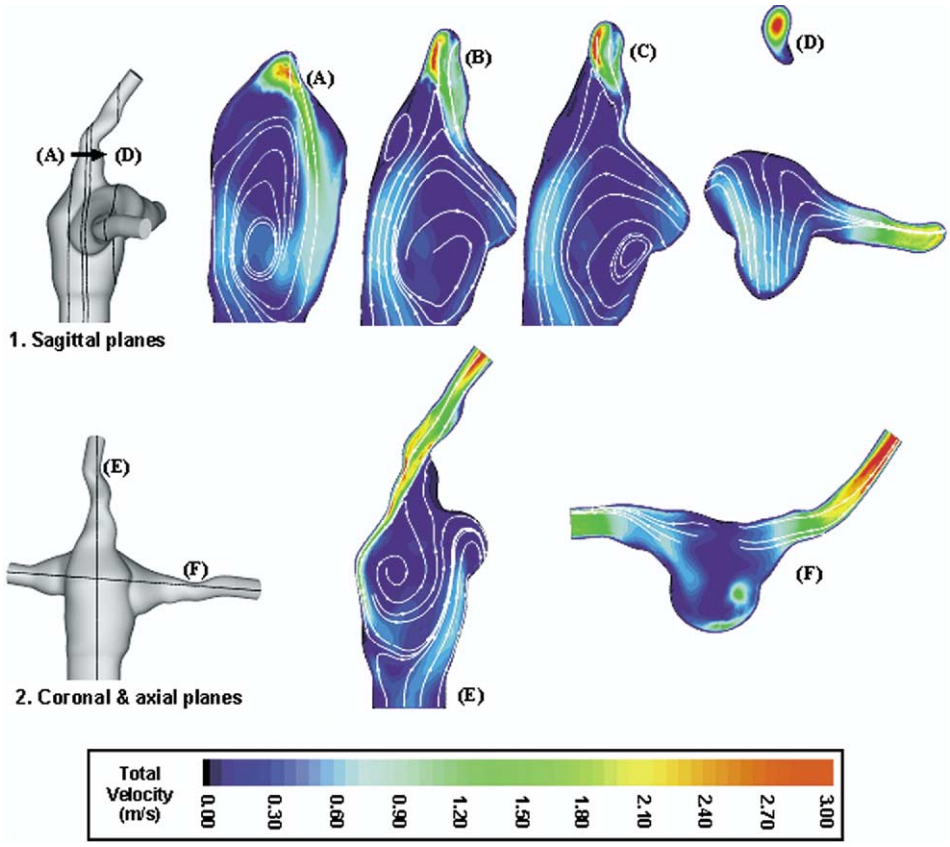

Fig 7. Assessment of the total velocity using computational fluid dynamic methods; at 3 L/min, 60/40 inferior vena cava to superior vena cava, and 50/50 left pulmonary artery to right pulmonary artery. The location of the sagittal (A to D), coronal (E), and axial (F) planes is shown in schematics 1 and 2.

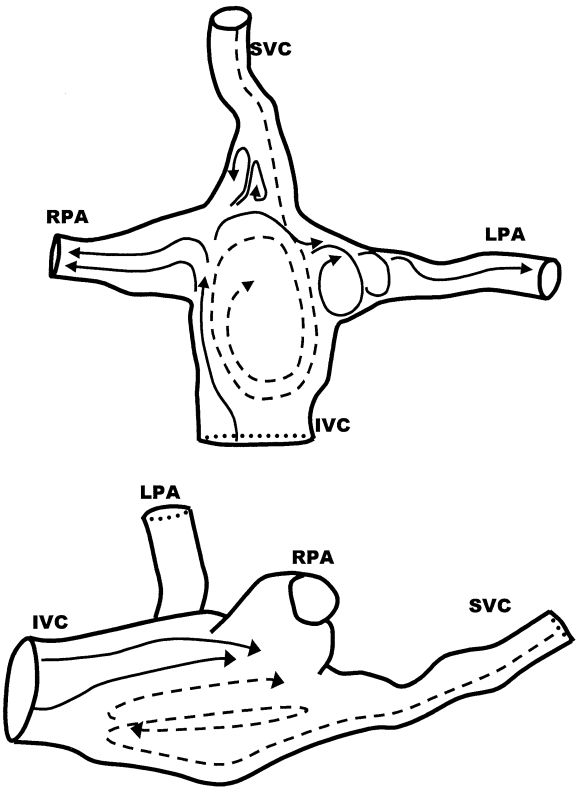

*Fig 8. Schematic of the flow structure in the intraatrial model at 1 L/min, 60/40 inferior vena cava to superior vena cava, and 70/30 left pulmonary artery to right pulmonary artery. (*IVC = *inferior vena cava;* LPA = *left pulmonary artery;* RPA = *right pulmonary artery;* SVC = *superior vena cava.)*

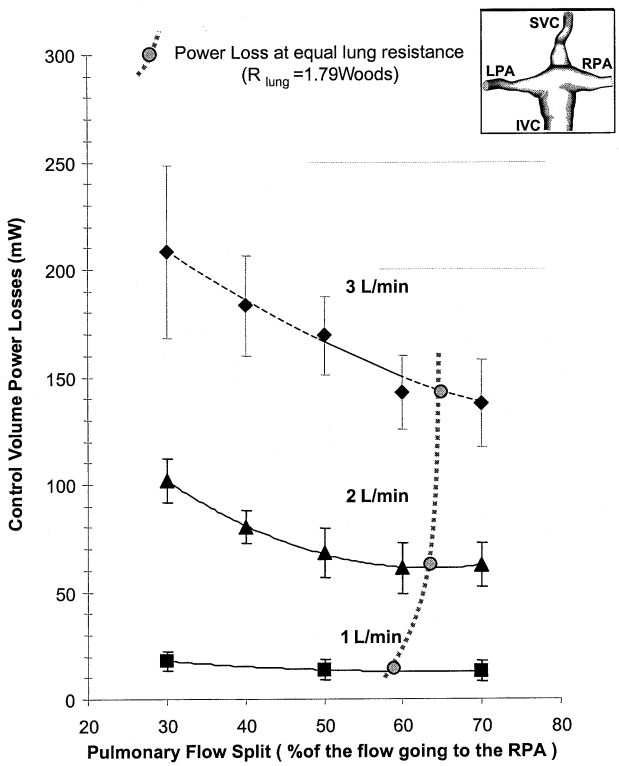

*Fig 9. Control volume power losses in the anatomic intraatrial model. At 3 L/min, fully developed turbulence took place in the left pulmonary artery (*LPA*) below 50% right pulmonary artery (*RPA*) and in the left pulmonary artery above 60% right pulmonary artery. (*IVC = *inferior vena cava;* SVC = *superior vena cava.)*

area was negligible when compared with the 600% to 700% increase that was observed when changing the vessel diameters of model 1 down to those of model 2. This may be explained by the fact that most of the energy is dissipated through viscous friction along the walls.

Contrary to model 1, an important clockwise recirculation was noted in the connection site of model 2 (Figs 2C, 2D) because of the difference between the LPA and RPA diameters. Computing the equal PVR points of each model underlined that asymmetric pulmonary diameters lead to uneven lung perfusion. Although the functioning point of model 1 was at about 50/50 RPA/LPA for all flow rates, model 2 and the anatomic model clearly favored right lung perfusion, with an equal PVR point around 70/30 RPA/LPA. Lung perfusion was found to be even more unbalanced as the cardiac output increased: in the anatomic model the equal PVR point corresponded to 59/41 RPA/LPA at 1 L/min versus 65/35 RPA/LPA at 3 L/min. In model 2, the uneven lung perfusion resulted from the asymmetry in vessel diameter between the LPA and RPA. In the anatomic model, it resulted from the combined asymmetries of the PA diameters and of their flaring rate.

Numerical results and experimental flow visualization confirmed the presence of secondary flow structures in the PAs of the anatomic and simplified models. Helical pulmonary flow as a result of the colliding caval flows has been observed in most TCPC models, from the simplest idealized glass models to more sophisticated numerical modeling [6, 14, 15]. It has a positive impact as it minimizes pulmonary flow separation and prevents the formation of stagnation regions at the entrance of the PAs. However, these secondary flow structures may also be one of the major sources of power losses as they increase the friction along the vessel walls. Increased disturbances in the connection area enforce the secondary flow structures in the PAs. The CFD pressure map (Fig 10) demonstrated that most of the pressure drops, and subsequently most of the losses, occurred at the entrance of the PAs. In the anatomic case studied here, the impact of helicity on the power losses was brought to an even higher level because of the rapid tapering of the arteries, which accelerated the flow along the walls, especially in the LPA, which tapered down faster than the RPA.

In the anatomic model, the vessels were flared to make up for the diameter mismatch with the large connection area. Rapid tapering of the vessels led to flow separation in the SVC and increased wall friction in the LPA. Ideally the transition between the connection area and the vessels should be as smooth as possible, but may be constrained by other vessels or organs. Avoiding large connection areas would also minimize the diameter mismatch.

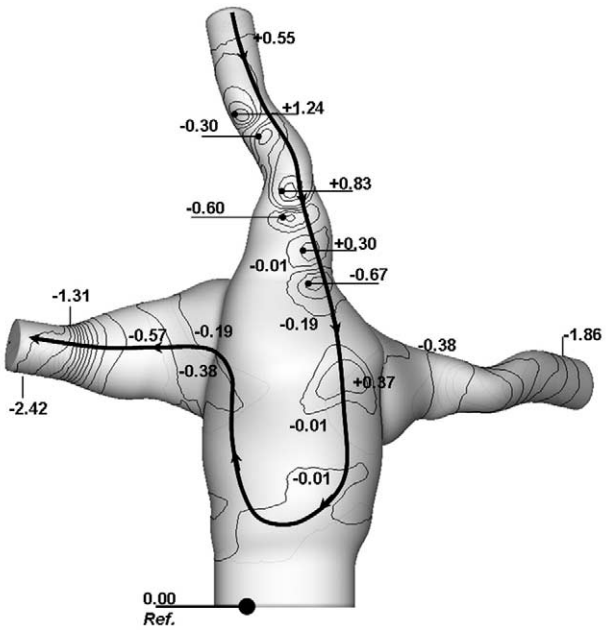

*Fig 10. Pressure distribution in the anatomical intraatrial model at 1 L/min; inlet flow split: 60/40 inferior vena cava to superior vena cava; outlet flow split: 70/30 left pulmonary artery to right pulmonary artery. Pressures are given in millimeters of mercury. Inferior vena cava pressure was chosen as the reference (*Ref.*).*

The intraatrial TCPC presented here was characterized by high power losses owing to (1) the absence of caval offset, (2) the large connection area, and (3) the dimension of the vessels. Most of the energy was dissipated in the PAs through wall friction. The diameter of the PAs is thus a crucial factor, which is especially relevant for patients with PA stenosis. The connection area should match the diameter of the connecting vessels as closely as possible because important dimension mismatch increased the flow disturbances at the center of the connection, and abrupt changes in vessel diameters yielded higher energy dissipation and flow separation with stagnant flow regions.

The main limitations of this study are that it features a single patient anatomy and uses rigid models. The compliance of the baffle and its motion when the single ventricle contracts are still unknown. The compliance provided by latex-type materials, such as Sylgard, may not have been any more relevant than noncompliant models.

The methodology proposed here focused on the geometric accuracy of the reconstructed vessels. It applies to any patient, and the reconstructed geometry can be modified on a computer and studied numerically and experimentally. Future endeavors include studying a larger number of patient anatomies, focusing on the variation among differing TCPC techniques, and directly comparing intraatrial and extracardiac connections. Additional factors such as flow pulsatility and wall compliance should be also addressed.

This work was supported by a BRP grant from the National Heart, Lung, and Blood Institute, HL67622. The glycerin was provided by P&G, Cincinnati, OH.

References

1. Fontan F, Baudet E. Surgical repair of tricuspid atresia. Thorax 1971;26:240–8.
2. Gersony D, Gersony W. Management of the postoperative Fontan patient. Progr Pediatr Cardiol 2003;17:73–9.
3. de Leval M, Kilner P, Gewillig M, Bull C. Total cavopulmonary connection: a logical alternative to atriopulmonary connection for complex Fontan operations. Experimental studies and early experiences. J Thorac Surg 1988;96:682–95.
4. Ensley A, Lynch P, Chatzimavroudis , Lucas C, Sharma S, Yoganathan A. Toward designing the optimal total cavopulmonary connection: an in vitro study. Ann Thorac Surg 1999;68:1384–90.
5. Liu Y, Pekkan K, Jones C, Yoganathan A. The effect of different mesh generation methods on computational fluid dynamic analysis and power loss assessment in total cavopulmonary connection. J Biomech Eng 2004;126:594–603.
6. Ryu K, Healy T, Ensley A, Sharma C, Lucas C, Yoganathan A. Importance of accurate geometry in study of the total cavopulmonary connection: computational simulations and in vitro experiments. Ann Biomed Eng 2001;29:844–53.
7. Migliavacca F, Dubini G, Bove E, de Leval M. Computational fluid dynamics simulations in realistic 3-D geometries of the total cavopulmonary anastomosis: the influence of the inferior caval anastomosis. J Biomech Eng 2003;125:805–13.
8. Hsia TY, Migliavacca F, Pittacio S. Computational fluid dynamic study of flow optimization in realistic models of the total cavopulmonary connection. J Surg Res 2004;116:305–13.
9. Yedavalli RV, Loth F, Yardimci A, et al. Construction of a physical model of the human carotid artery based upon in vivo magnetic resonance images. J Biomech Eng 2001;123:372–6.
10. de Zélicourt D, Pekkan K, Kitajima H, Frakes D, Yoganathan A. Single-step stereolithography of complex anatomical models for optical flow measurements. J Biomech Eng. In Press.
11. Sharma S, Goudy S, Walker P, et al. In vitro flow experiments for determination of optimal geometry of total cavopulmonary connection for surgical repair of children with functional single ventricle. J Am Coll Cardiol 1996;27:1264–9.
12. Pekkan K, de Zélicourt D, Ge L, et al. Flow physics driven CFD modeling of complex anatomical flows—a TCPC case study. Ann Biomed Eng. In press.
13. Khunatron Y, Shandas R, DeGroff C, Mahalingam S. Comparison of in vitro velocity measurements in a scaled total cavopulmonary connection with computational predictions. Ann Biomed Eng 2003;31:810–22.
14. Bolzon G, Pedrizzetti G, Grigioni M, Zovatto L, Daniele C, D'Avenio G. Flow on the symmetry plane of a total cavopulmonary connection. J Biomech 2002;35:595–608.
15. Migliavacca F, de Leval MR, Dubini G, Pietrabissa R, Fumero R. Computational fluid dynamic simulations of cavopulmonary connections with an extracardiac lateral conduit. Med Eng Phys 1999;21:187–93.